https://doi.org/10.1016/j.nanoen.2023.109238

A bubble energy generator featuring lubricant-impregnated surface with high durability and efficiency

Xiantong Yan[a], Yuxin Song[b], Huanxi Zheng[b], Hongzhi Cui[a], Zuankai Wang[b,*], Wanghuai Xu[c,*]

a. State Key Laboratory of Subtropical Building and Urban Science (SZU), Key Laboratory for Resilient Infrastructures of Coastal Cities (MOE), College of Civil and Transportation Engineering, Shenzhen University, Shenzhen, China

b. Department of Mechanical Engineering, The Hong Kong Polytechnic University, Hong Kong, China

c. Department of Electrical and Electronic Engineering, The Hong Kong Polytechnic University, Hong Kong, China

*Corresponding author. email: wanghuai.xu@polyu.edu.hk (W. Xu); email: zk.wang@polyu.edu.hk (Z. Wang).

Abstract

Harvesting bubble energy emerges as a potential sustainable solution to harness tremendous marine energy sources. Yet, current bubble energy generators are susceptible to unstable performance owing to the degradation of the physiochemical properties of surface materials under the harsh underwater environment such as surface fouling and wetting transition. Here, we report the design of bubble energy generators featuring the cooperative integration of a slippery lubricant-impregnated porous surface and transistor-inspired architecture, referred to as SLIPS-TBG, that can generate electricity from moving bubbles with high stability in submerged conditions. In this design, the slippery and configurable lubricant layer serves as not only a smooth and mechanically stable surface for bubble transport but also a protective layer preventing the underlying solid materials from direct contact with the external harsh environment. Together with the transistor-inspired architecture, the SLIPS-TBG can deliver a stable electric output of 26.4 V, an instantaneous peak power density of 58.6 W m^{-3} from continuous bubble impingement in water media, even in extreme conditions involving mechanical abrasion and corrosion. We envision such a design represents a significant step toward real-life applications for bubble-based energy harvesting.

Keywords: Bubble energy harvesting, Slippery liquid surface, durability.

1. Introduction

Bubbles are of fundamental interest and importance in many applications, including serving as a medium to reduce energy consumption in drag reduction in marine [1, 2], being carriers to enhance energy transfer in boiling heat transfer [3, 4], and targeted cancer diagnosis [5]. However, unlike water energy harvesting that has been extensively explored [6-16], the substantial potential energy abounding in underwater bubbles remains largely untapped. Conventional techniques such as reverse electrowetting [17], triboelectric nanogenerator [18-23], electromagnetic generator [24-27], and piezoelectricity [28] are limited by the need of additional energy input, super-large bubble size, or low output voltage. Recently, a transistor-inspired bubble energy generator (TBG) [29] from Wang's group has been developed for efficiently harvesting energy from small bubbles. The fundamental mechanism of TBG lies in the efficient transition between the liquid/solid interface and gas/solid interface upon the contact between the bubble and the generator surface, as well as the transistor-inspired design that allows for efficient charge transfer and an electric output at least one order of magnitude higher than conventional techniques.

Despite extensive progress, operating in underwater environments, current TBGs are susceptible to low stability and performance decline during long-term operation, mainly owing to the vulnerable nature of solid generator surfaces [30] in harsh underwater environments. First, the effective interfacial transition requires a solid surface to be moderately hydrophobic for balancing the fast spread and rapid detachment of bubbles whereas suppresses the formation of continuous water film on the surface. However, the hydrophobic surfaces lead to inferior resistance to the adhesion of microorganisms that are ubiquitous in underwater conditions [31]. As a result, the interfacial charge transfer for efficient electricity generation would be undermined. Second, solid hydrophobic surfaces suffer from the unwanted wetting transitions caused by hydrodynamic impact in underwater environments [32, 33], leading to the failure of water-repellency property of the surface for continuous electricity generation. More challenges emerge in harsh environments involving corrosion, mechanical wear, abrasion, and impact, where the solid surfaces made of thin membrane can be easily cracked [34], causing the performance decline or even fatal short-circuit problems owning to exposure of underlying

electrode to surrounding water.

Herein, we report the design of a SLIPS-TBG that can deliver efficient electric output performance from underwater bubbles while maintaining long-term stability and robustness in submerged environments. The liquid lubricant surface of SLIPS not only allows for the efficient transition between the SLIPS/water interface and SLIPS/gas interface upon bubble contact for electricity generation, but also is inherently smooth, water repellency, antifouling, and mechanically stable. Meanwhile, the transistor-inspired architecture can fully harness the interfacial charges at the SLIPS/water interface for electricity generation. The synergy between these features of SLIPS-TBG collectively results in an electric output of 26.4 V with a small bubble of 0.1 ml even in various hash conditions including mechanical abrasion, strong corrosive solutions, and biofouling. This work not only contributes to expanding the bubble energy harvesting techniques to more diverse interfacial scenarios but also represents a significant step toward the real-life applications of submarine energy harvesting.

2. Results

The SLIPS-TBG is designed to consist of a SLIPS layer, a bottom (indium tin oxide, ITO) electrode on the glass substrate, and the other electrode (Pt) positioned in water (Fig. 1A). As shown in Fig. 1B, the SLIPS layer is engineered by impregnating an oil-based lubricant (DuPont Krytox GPL 103, dielectric constant ≈ 2.1, surface tension $\gamma \approx 16$ - 20 mN/m, Fig. S1) into a porous superhydrophobic (SHS) polytetrafluoroethylene (PTFE) membrane with the aid of capillary wicking effect, transforming porous PTFE membrane into a liquid, slippery, and transparent film (Fig. 1C-E). Notably, the intrinsic softness of the SLIPS layer enables the construction of SLIPS-TBG on a flexible substrate (Fig. S2), preferential for further integration with other devices. Moreover, from the architecture perspective, the design of SLIPS-TBG is analogy to that of an electronic transistor, with the ITO electrode and SLIPS layer covalently serving as the source terminal, the Pt electrode positioned in water acting as the drain terminal, and the moving bubble behaving like a gate terminal. Such a transistor-inspired electrode design enables efficient charge transfer in submerged environments through the utilization of abundant electric charges pre-stored in the SLIPS layer.

We first examine the bubble affinity and mobility on SLIPS-TBG in the submerged

environment. As shown in Fig. 1F, the SLIPS layer of SLIPS-TBG exhibits an apparent bubble contact angle (BCA) of 75° in water, which is smaller than the BCA of 85° on the porous solid SHS, suggesting higher bubble affinity of SLIPS-TBG over the counterpart without the lubricant (SHS-TBG). Such a result is contrary to the common perception that a hydrophobic flat surface is usually less aerophilic than a SHS [35, 36]. The reason for this intriguing phenomenon may be that the SLIPS layer features a molecular-level smooth surface that facilitates the spread of a bubble with low interfacial friction [37]. In contrast, the SHS hinders the spread of bubble owing to the pinning effect at the three-phase contact line rendered by the porous structure [38]. This striking contrast is also revealed when we compare the bubble mobility of SLIPS-TBG and SHS-TBG in underwater environments. As shown in Fig. 1G, on the SLIPS with a tilting angle of ~45°, a bubble of 0.1 ml releasing from a nozzle 18.0 mm below the device contacts and subsequently departs from the surface in 68 ms without apparent velocity variation. Notably, the bubble impinging on the SHS-TBG suddenly decelerates upon contact with the surface and then moves slowly on the surface owing to the large surface friction, taking 321 ms for full departure from the surface. Taken together, SLIPS-TBG shows both superior bubble affinity and mobility, both of which are preferential for efficient electricity generation.

A glimpse of the advantages of the SLIPS-TBG in electricity generation is shown in Fig. 1H. A bubble of 0.1 ml released from a nozzle 18.0 mm below the device can generate a voltage of 26.4 V, which is ~6 folds higher than that generated by the SHS-TBG. The instantaneous peak power density of SLIPS-TBG is 58.6 W m^{-3} under a load resistance R_L of 100 megohms (Fig. S3), which is ~40 times higher than that of the control device without the lubricant impregnation. We also note that the output performance of SLIPS-TBG is not sensitive to specific electrode parameters, such as materials, sizes, and spatial distributions. As shown in Fig. S4, the output voltage measured from SLIPS-TBGs with varying electrode parameters fluctuates in a small range between 25.3 V and 26.4 V, suggesting its excellent adaptability for energy harvesting in dynamic and complex environments. However, the parameters affecting bubble/SLIPS interaction, such as tilting angle and bubble shape defined by aspect ratio, $\alpha = (a - b) / a$, where a and b are the semi-major and semi-minor axis of the rising bubble, respectively, have a significant impact on the output voltage of SLIPS-TBG. It was found that

the output voltage of SLIPS-TBG achieves the maximum at a tilting angle of 45° (Fig. S5) and shows a gradual increase from 4.6 V to 26.4 V as the bubble aspect ratio increases from ~0.02 to ~0.7 (Fig. S6). Thus, these results including the irrelevance of electrode parameters and the relevance of bubble aspect ratio as well as titling angle collectively indicate that the excellent output performance should result from the interaction between SLIPS-TBG and impinging bubbles.

To probe the fundamental mechanism responsible for the enhanced output performance, we examine how the bubble/SLIPS interaction induces the electric output. Fig. 2A shows the synchronization between the bubble dynamics on SLIPS and the voltage signal (Video S1). The bubble first spreads, then recoils, and finally departs from the surface with a contact time of ~68.0 ms on the SLIPS, which is accompanied by the transition from a water/SLIPS interface into a gas/SLIPS interface that is featured by a time-dependent variation in the bubble/SLIPS interface area. These processes initiate from the attachment of an approaching bubble on the SLIPS through draining the water film between them via a short-ranged hydrophobic attraction [39]. Upon the attachment of the bubble on the SLIPS at 0 ms, the output voltage starts to increase from zero and reaches the peak value at ~19.3 ms when the bubble is still spreading. As the bubble reaches a maximum spreading diameter of ~7.4 mm at 28 ms, the output voltage drops to zero. Subsequently, the voltage signal turns into a negative value as the recoiling of the bubble and returns to 0 V when the bubble completely departs from the SLIPS at 68 ms. Notably, during the whole electricity generation process, the lubricant layer on SLIPS keeps an integral configuration without rupture according to the lubrication approximation analysis (Fig. S7).

The fundamental mechanism of the TBENG can be explained in Fig. 2B. The Pt electrode positioned in water connects the ITO electrode, water, and the SLIPS layer into a closed-loop electric circuit. Prior to the contact of the bubble, the surface charges pre-stored on the SLIPS are electrostatically screened by the ambient water. In this circumstance, there is no charge transfer between the ITO electrode and the Pt electrode. As the bubble contacts the SLIPS-TBG, the SLIPS layer gradually exposes to the air owing to the drainage of surface water driven by the bubble. Such a process is accompanied by a transformation from liquid/SLIPS interface to gas-SLIPS interface whereas the surface charges on the SLIPS layer become electrically

unbalanced, leading to charge transfer from the water to the ITO electrode. Subsequently, the recoiling of the bubble restores the electrostatic screening of water on the SLIPS layer, driving the backflow of electric charges from the ITO electrode to water and a new cycle starts. This physical rationale can also be convinced by simulating the electrical potential evolution during this process (COMSOL Multiphysics 5.4, Fig. S8). Particularly, a potential difference with a maximum of 48.3 V is established between the water and the SLIPS layer when the bubble separates the water and SLIPS, which drives charge transfer between the Pt electrode and water. The simulation result aligned well with our proposed mechanism.

The superior electricity generation of SLIPS-TBG is simultaneously accompanied by enhanced stability, especially under extreme conditions involving biofouling, corrosive liquid, or even mechanical abrasion. As shown in Fig. S9, after being immersed in an underwater environment that is suitable for green algal propagation, the SLIPS-TBG sustains a clean and smooth surface for a long time of 30 days while the SHS-TBG is contaminated by a layer of yellow biofouling approaching 90% of its surface area (Fig. 2C). This is because the presence of SLIPS layer imparts a smooth and dynamic oil/water interface, which can prevent the anchor of microorganisms via pili and other cellular mechanisms as those on a solid surface [40]. Moreover, the lubricant liquid of our SLIPS-TBG is immiscible with the aqueous water medium, making it difficult for microorganisms to penetrate, even with bacterial surfactant production [41]. As a result, the SLIPS-TBG generates an output voltage close to the initial value, which is in striking contrast to the SHS-TBG losing its efficacy owing to the coverage of biofouling that blocks bubble/SHS-TBG interaction (Fig. 2D). In addition, the adoption of SLIPS layer also confers SLIPS-TBG with strong resistance to environmental corrosion (Fig. S10). As shown in Fig. 2E, the voltage output of SLIPS-TBG sustains after being immersed in an acid solution with a pH value varying from 1 to 7 for 30 min, and the value just moderately declines when the pH value surpasses 7. Moreover, we also found that the SLIPS layer of SLIPS-TBG exhibits a self-configuration behavior [42, 43] after the mechanical damages, ensuring a robust voltage output of SLIPS-TBG under friction. Specifically, we abrade the SLIPS surface with a sandpaper of 100 meshes with a 50-gram weight on the top to induce several apparent defective sites on the SLIPS layer as shown in Fig. S11. Interestingly, the SLIPS-TBG gradually restores its original smooth surface as the surrounding lubricant

spontaneously flows into the defective sites and the measured output voltage from self-respired SLIPS-TBG is comparable to the initial electrical performance of the device (Fig. 2F), further demonstrating the excellent robustness of SLIPS-TBG.

The manifestation of stable electric generation from SLIPS-TBG also demands the elegant regulation of the lubricant thickness and viscosity. As shown in Fig. 3A, given the fixed lubricant viscosity at 1535 cSt, the output voltage of SLIPS-TBG exhibits an increasing trend from 4.3 V to 26.4 V with the increased lubricant thickness from 0 μm to 5.25 μm, which can be attributed to the enhanced bubble mobility on the SLIPS. However, further increasing the lubricant thickness to 12.8 μm leads to a remarkable reduction of voltage output to 6.2 V. This is because the thick lubricant layer hinders the efficient electrostatic induction between the water and the surface charges on SLIPS, declining the charge transfer between the electrode and the water. Moreover, the output voltage of SLIPS-TBG is also regulated by the lubricant viscosity (Fig. 3B). The output voltage increases from 5.6 V to 26.4 V as lubricant viscosity increases from 17.4 cSt to 1535 cSt. Such a viscosity-dependent output probably results from the enhanced retention capability of viscous lubricant to keep the optimal thickness. It is noted that the output voltage keeps constant despite varying bubble frequency from 2 Hz to 8 Hz (Fig. 3C), suggesting the independence of electricity generation on the bubble frequency, which is beneficial for improving the overall energy generated from the bubbles.

The electricity generation of SLIPS-TBG can be further improved when the bubble/SLIPS-TBG interaction occurs in the air environment, in which the fast bubble collapse remarkably accelerates the charge transfer and leads to enhanced output (Video S2). Snapshots of bubble dynamics in Fig. 3D show that a bubble in contact with the SLIPS-TBG above in the air takes 6.3 ms to collapse, representing an 84.3% reduction in the bubble departure time. Moreover, without water confinement and water screening, the SLIPS-TBG deliveries an output voltage of approximately 40 V (Fig. 3E) in the air, representing a 51.5% enhancement in the output voltage as compared to that of the SLIPS-TBG in an underwater environment. Such an output rivals or outperforms most previous studies related to electricity generation at gas/liquid interface (Table S1), suggesting the generality of the design of our SLIPS-TBG and the corresponding working mechanism.

Enhancing the stability of electricity generation of SLIPS-TBG imparts broad application

scenarios, especially in offshore and off-grid settings. For example, the SLIPS-TBG can be used to detect the initialization of the reaction and evaluate the subsequent reaction rate based on the measured voltage from the generated gas bubbles (Fig. 4A). As shown in Fig. 4B, the values of the generated voltages are positively related to the volumes of the bubbles produced by the reactions. These data provide an institutive estimation of the reaction rate and can be used for calculating the total volume of the generated gas phase. Furthermore, the excellent electricity generation capability of the SLIPS-TBG is also suitable for off-grid regions where power supply is not achievable. The electricity generated from bubbles can be stored in capacitors (Fig. 4C), serving as a sustainable, clean, and real-time source for powering underwater communication devices. As shown in Fig. 4D, we designed a bubble-energy-driven communication system for information encryption transmission in submarine environments. When the system works at "off" state, the display screen is totally black, and no light can transmit through it (Fig. 4E). In this regard, the privacy information designed in the QR code integrated with the display screen is well protected. When the system is switched on (Fig. 4F), a QR code containing privacy information can be clearly identified by scanning equipment. Notably, the transition from the "on" state to the "off" state and subsequent restoration to "off" state (Fig. 4G) can be immediately achieved within less than 1 s by simply switching off the control electric circuit. Such a feature is highly desirable for information protection in emergent situations.

3. Discussion

Fundamentally, through the cooperative integration of a transistor-inspired architecture and a SLIPS layer, we designed a previously undefined bubble energy generator based on gas-SLIPS interaction in submarine environments. The key point lies in the design of a transistor-inspired architecture that allows for efficient charge transfer in submerged conditions and the SLIPS layer that endows anti-biofouling, anti-corrosion, and self-configurable capability, resulting in an efficient, continuous, and robust electricity generation occurring at the gas-liquid interface. From the output performance perspective, the transistor-inspired architecture of SLIPS-TBG enables a stable output of 26.4 V and an energy conversion efficiency of ~0.6% with a small bubble of 0.1 ml, rivaling or outperforming most previous gas/liquid-based generators. From

the perspective of device structure, the SLIPS-TBG possesses a soft and dynamic surface, rendering a duration of bubble/SLIPS-TBG (68.0 ms) interaction that is about 1.5 times longer than that of a TBG (40.0 ms). Thus, although the output voltage of SLIPS-TBG is almost 1.5 times lower than that of a solid-based TBG (40.0 V) [29], the SLIPS-TBG exhibits an energy conversion efficiency only slightly lower than that of a TBG (~1%).

Moreover, compared to a liquid-based droplet energy generator that achieves the best performance in ambient humidity[44], our SLIPS-TBG device can work in submerged environments and the open-system design of the SLIPS-TBG eliminates the need for sealed components in submerged conditions, which extends the application scope of underwater energy harvesting technology. Probably more importantly, the design of SLIPS-TBG that combines the merits of a transistor-inspired structure and a gas-liquid interface is another breakthrough after the high-efficiency power generation of the gas-solid interface [29], solid-liquid interface [8, 9], solid-solid interface [45], and liquid-liquid interface [46], which proves the universality of a transistor-inspired architecture design. We envision that the innovation of our SLIPS-TBG will spur new thinking in designing versatile energy devices that can be used as a clean and robust alternative in various working environments.

Material and methods

Materials

Acetone (RCI Labscan, 99.5%), ethanol (Sigma Aldrich, 97%), nitric acid (Sigma Aldrich, 70%), hydrochloric acid (Sigma Aldrich, 37%), deionized water, and DuPont Krytox GPL 103, 105, and 107 oil were used without further purification. The indium tin oxide (ITO) glasses with dimensions of 60 mm × 30 mm × 1.1 mm and ITO thickness of 10 μm were purchased from Huanan Xiangcheng Company, China. To achieve favorable electricity generation and the stability of the lubricant layer, porous PTFE membranes (PTU023001, Sterlitech Corporation, US) with a thickness of ~ 20 μm, average pore size of ~ 200 nm, and porosity of ~ 85%, were chosen. Platinum (Pt) electrode with size of 5 mm × 5 mm × 0.2 mm was purchased from Jiang Su Xin Chen Company, China.

Fabrication

We fabricate the SLIPS-TBG device by the following steps. First, an ITO glass was ultrasonically cleaned in acetone and ethanol for 10 min. Second, the ITO glass was gently covered by a PTFE membrane followed by the ethanol wetting treatment for a good affinity between PTFE and ITO glass. Third, after the ethanol completely evaporated, several drops of DuPont Krytox GPL oil with predesigned volume V and viscosity μ were dripped onto the PTFE membrane using a high-precision syringe pump. The lubricant liquid possesses a low dielectric constant for reducing the electrical screening effect on the surface charge, high wetting affinity with PTFE membrane, immiscibility with most liquids, high-temperature stability, low vapor pressure, and chemical inertness. Thereafter, we horizontally placed the samples on a flat table for 12 hours to allow spontaneous impregnation of the lubricant. Last, as the pores of PTFE membrane were uniformly filled by the lubricant oil, we connected the ITO glass underneath the SLIPS layer with a Pt electrode that was positioned in water. For comparison, control devices without the impregnation of lubricant, termed SHS-TBG, are also fabricated. The thickness h of the lubricant layer was controlled by the volume of lubricant according to the area A of PTFE.

Characterization and electric measurement

Gas bubbles with a frequency of 5.0 Hz and a fixed volume V_b of 0.1 ml were produced by an

air pump in water. To control V_b, the gas flow (10.0 ml/min) in the air pump, the diameter (4.0 mm) of the dispenser, and the water depth (18.0 mm) were set to be fixed. The contact and detachment dynamics of gas bubbles were recorded by a high-speed camera (Photron FASTCAM SA4) with a typical recording speed of 3000 frames per second. We measured the optical transmittance of SLIPS-TBG and SHS-TBG in the visible light range (400-800 nm) using a Perkin Elmer Lambda 35 UV-Vis spectrometer. The output voltage of SLIPS-TBG and SHS-TBG was measured using an oscilloscope (Rohde and Schwarzrte, RTE1024) equipped with a high-impedance (100 megohms) probe. If not specified, all experiments were conducted at room temperature of 23 ℃ in tap water with an ion concentration of 3.1 mM and the sample was fixed at a tilting angle of ~ 45°.

Calculation of power, energy, and energy conversion efficiency

The instantaneous peak power P generated from a bubble impinging on SLIPS-TBG is calculated by $P = V_p^2/R_L$, where R_L is load resistance and V_p is the instantaneous peak value of measured voltage. The energy generated from a bubble is calculated by $E = \int_0^\tau \frac{V^2(t)}{R_L} dt$, where V(t) is the measured time-evolved voltage generated from a bubble.

The energy conversion efficiency η of SLIPS-TBG, defined as the harvested electrical energy E relative to the input energy E_{in} (buoyancy work) of an impinging bubble, is expressed as

$$\eta = \frac{E}{E_{in}} = \frac{E}{\rho V_b g s}$$

Where ρ, g, V_b, and s are the water density (1000.0 kg/m^3), gravitational acceleration (9.8 m/s^2), bubble volume (0.1 ml), and water depth (18.0 mm), respectively.

Anti-biofouling test

We conducted the anti-biofouling test in a transparent glass tank with a dimension of 50 cm × 27 cm × 30 cm that mimics the ecosystem of a natural stream. There are 40-liter tap water in the tank and an Eheim 250 filter is used to drive the flow of water. 10 *pseudorasbora parva* bought from the local market of Hong Kong were added to the water tank acting as the consumer and 5 ml of high-purity commercial nitrobacteria was added to the water serving as the decomposer. To provide the light needed for the cultivation of the microorganisms in water,

we adopted a light emission diode lamp of 100 W with a wavelength range of 400-750 nm to simulate the visible light. After stewing the water in the tank for 7 days, the SLIPS-TBG and SHS-TBG samples with a dimension of 30 mm × 30 mm × 1.1 mm were vertically placed on the bottom of the glass tank and radiated by the light emission diode lamp for 7 hours per day for 30 days. The anti-biofouling performance is characterized by comparing the coverage of the biofouling on the sample surface and the output performance of SLIPS-TBG and SHS-TBG before and after biofouling treatment are also compared.

CRediT authorship contribution statement

Xiantong Yan: Conceptualization, Methodology, Formula analysis, Investigation, Writing – original draft. **Yuxin Song**: Resources, Investigation, Formula analysis. **Huanxi Zheng**: Resources, Formula analysis. **Hongzhi Cui:** Resources, Writing - review & editing. **Zuankai Wang**: Conceptualization, Methodology, Supervision, Writing - review & editing. **Wanghuai Xu**: Resources, Methodology, Supervision, Writing – review & editing.

Declaration of Competing Interest

The authors declare that they have no known competing financial interests or personal relationships that could have appeared to influence the work reported in this paper.

Data availability

All data is available in the main text or the supplementary materials.

Acknowledgements

We acknowledge financial support from the Shenzhen Science and Technology Innovation Council (no. JCYJ20200109143206663), Shenzhen-Hong Kong-Macau Science and Technology Program (no. SGDX2020110309300502), Research Grants Council of Hong Kong (no. C1006-20WF, no. SRFS2223-1S01, no. PDFS2122-1S02), the National Natural Science Foundation of China (no. 51975502), the Innovation and Technology Council (no. GHP/092/20GD), the National Natural Science Foundation of China (no. 52308270), the China Postdoctoral Science Foundation (no. 2022M722189).

Figures

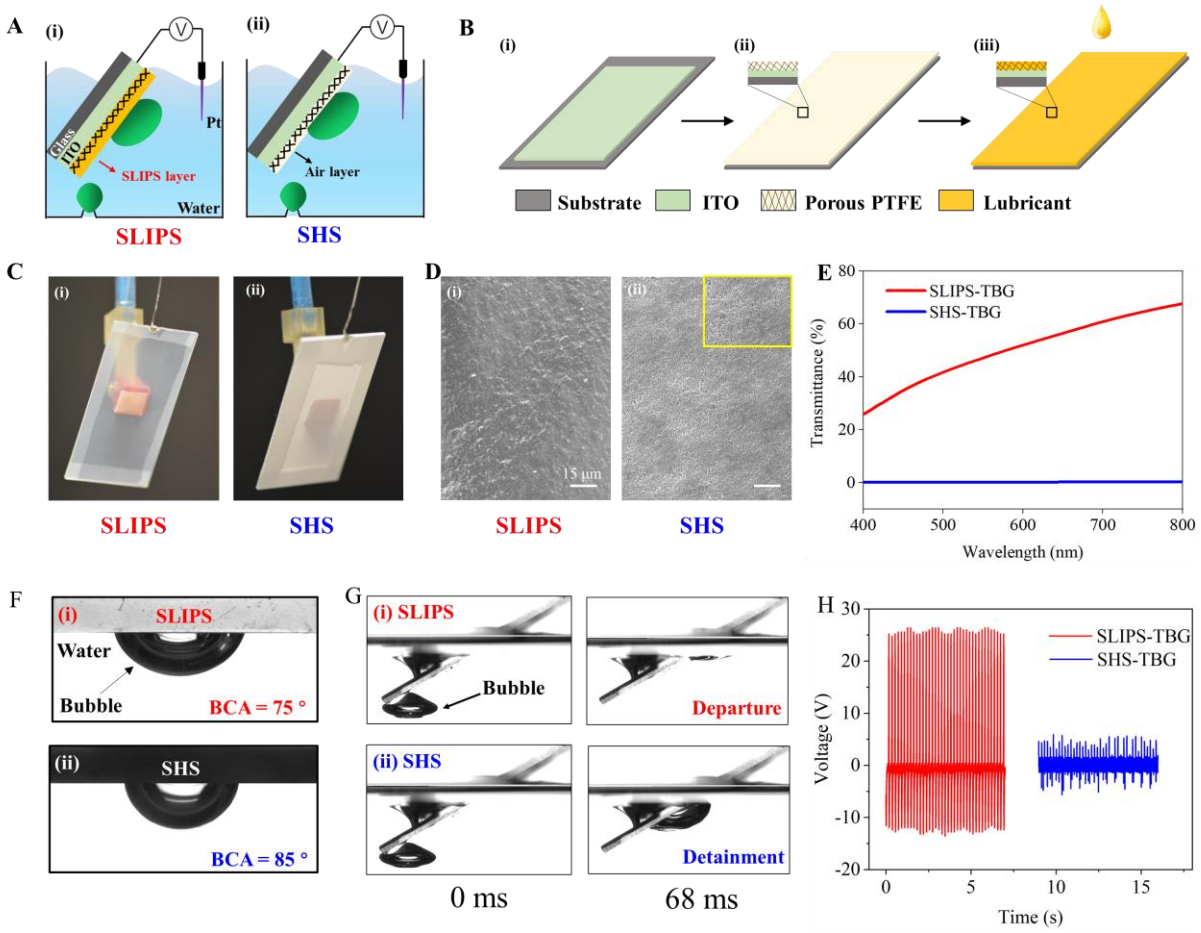

Figure 1. Design and realization of the SLIPS-TBG. A, Schematic comparison of the design of the SLIPS-TBG and the SHS-TBG. B, Schematic drawing showing the fabrication process of the SLIPS-TBG fabrication process. C, Photography of an as-fabricated SLIPS-TBG and the SHS-TBG. D, Comparison of SEM images of SLIPS and SHS. After infusing with the lubricant, the PTFE membrane with nanoscale porous fiber-like textures becomes smooth and liquid-like without visible pores, indicating the replacement of air pockets with the liquid lubricant. E, Comparison of optical transmittance between SLIPS-TBG and SHS-TBG. F, Optical images showing the bubble contact angles on the surfaces of the SLIPS-TBG and SHS-TBG. G, Comparison of bubble mobility on the surface of the SLIPS-TBG and SHS-TBG. H, Comparison of the open-circuit voltage of the SLIPS-TBG with that of the control device.

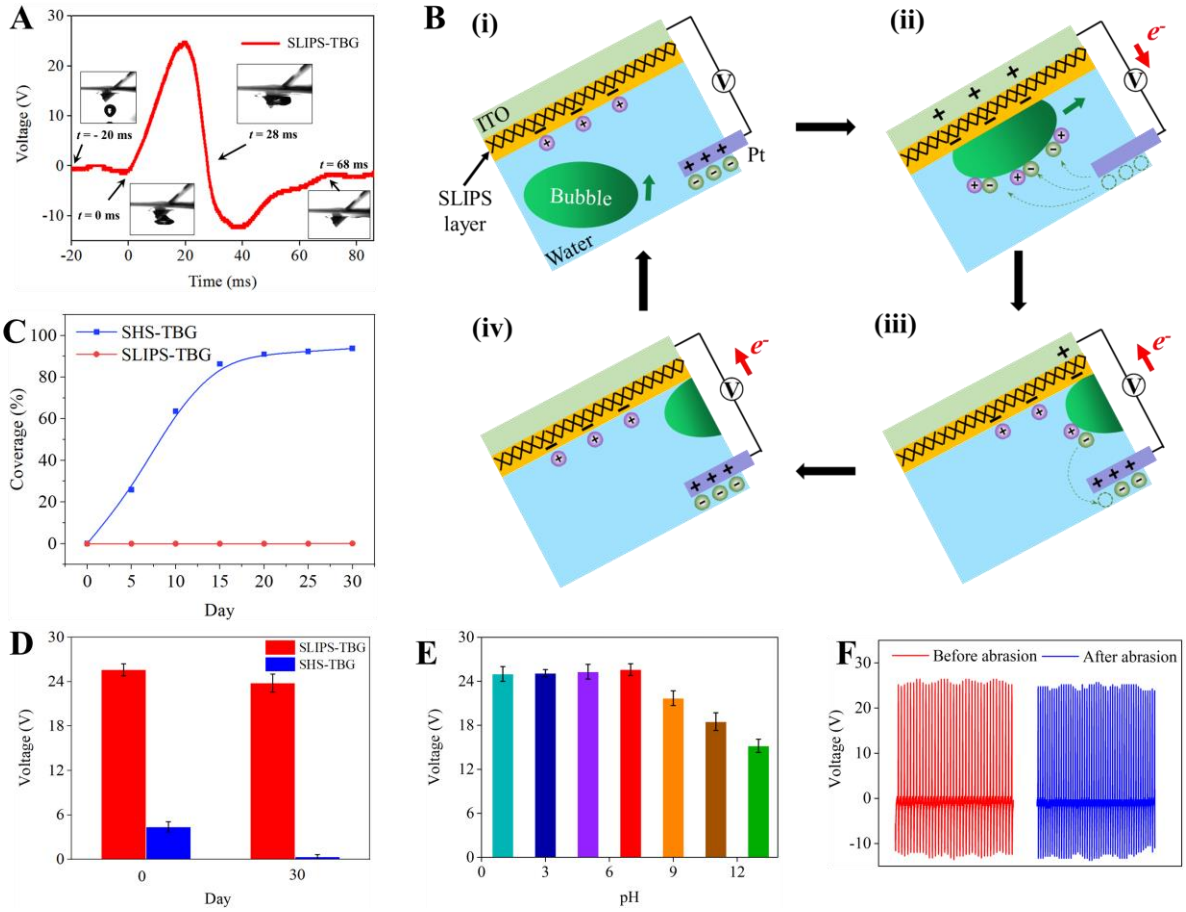

Figure 2. Working mechanism and stability of the SLIPS-TBG in harsh conditions. A, Time-dependent voltage response *V* and the corresponding bubble dynamics during bubble SLIPS interactions. B, Schematic drawing of working mechanism and corresponding charge transfer during bubble/SLIPS interaction. C, Calculated bio-fouling coverage area ratio on the SLIPS-TBG and SHS-TBG as a function of the immersion time. D, Variation of output voltage measured from the SLIPS-TBG and SHS-TBG before and after immersed in simulated natural water for 30 days. E, Variation of output voltage measured from the SLIPS-TBG after immersed in corrosive solutions with various pH values. F, Comparison of output voltage measured from the SLIPS-TBG before and after being abraded by sandpaper.

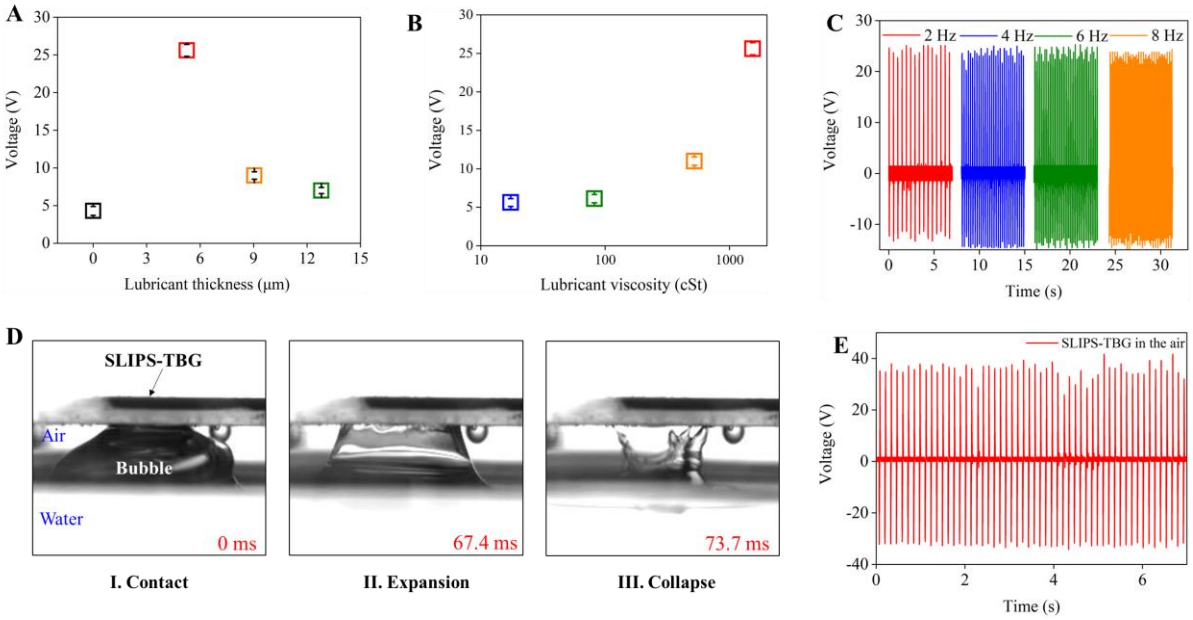

Figure 3. Generality of the SLIPS-TBG. A-B, Output voltages of SLIPS-TBG as a function of lubricant thickness and viscosity. C, Variation of output voltages of SLIPS-TBG from the bubble with various frequencies. D, Snapshots showing the accelerated bubble contact, expansion, and collapse dynamics in the air. E. Output voltage of the SLIPS-TBG with an individual bubble in the air reaches up to ~40 V.

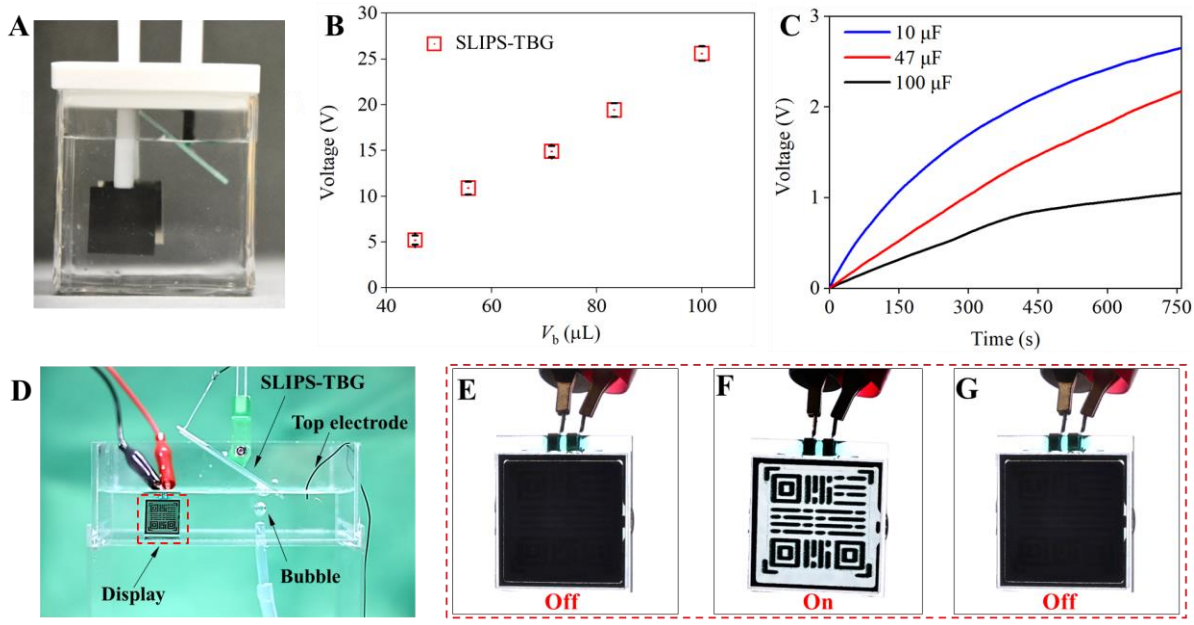

Figure 4. Demonstrations of the SLIPS-TBG. A, The SLIPS-TBG can be integrated with a gas emission reaction chamber for monitoring the initiation and reaction rate. B, Peak value of the output voltage is positively related to the volume of the generated bubbles, which can be used as an indicator for estimating the gas emission rate. C, Charging capability of the SLIPS-TBG under various capacitors. D, A SLIPS-TBG device successfully powers a light valve for information encryption transmission in submarine environments. E-G, Fast switch between off state and on state within 1 s.

Reference

[1] S.L. Ceccio, Friction drag reduction of external flows with bubble and gas injection, Annu. Rev. Fluid. Mech. 42 (2010) 183-203. https://doi.org/10.1146/annurev-fluid-121108-145504.

[2] S.R. Gonzalez Avila, D.M. Nguyen, S. Arunachalam, E.M. Domingues, H. Mishra, C.D. Ohl, Mitigating cavitation erosion using biomimetic gas-entrapping microtextured surfaces (GEMS), Sci. Adv. 6 (2020) eaax6192. https://www.science.org/doi/full/10.1126/sciadv.aax6192.

[3] X. Liang, V. Kumar, F. Ahmadi, Y. Zhu, Manipulation of droplets and bubbles for thermal applications, Droplet 1 (2022) 80-91. https://doi.org/10.1002/dro2.21.

[4] C. Li, Z. Wang, P.I. Wang, Y. Peles, N. Koratkar, G. Peterson, Nanostructured copper interfaces for enhanced boiling, Small 4 (2008) 1084-1088. https://doi.org/10.1002/smll.200700991.

[5] A. Bar Zion, A. Nourmahnad, D.R. Mittelstein, S. Shivaei, S. Yoo, M.T. Buss, et al., Acoustically triggered mechanotherapy using genetically encoded gas vesicles, Nat. Nanotechnol. 16 (2021) 1403-1412. https://doi.org/10.1038/s41565-021-00971-8.

[6] W. Xu, H. Zheng, Y. Liu, X. Zhou, C. Zhang, Y. Song, et al., A droplet-based electricity generator with high instantaneous power density, Nature 578 (2020) 392-396. https://doi.org/10.1038/s41586-020-1985-6.

[7] M. Liao, W. Xu, Y. Song, Z. Pan, H. Zheng, Y. Li, et al., An integrated electricity generator harnessing water and solar energy featuring common-electrode configuration, Nano Energy 116 (2023). https://doi.org/10.1016/j.nanoen.2023.108831.

[8] L. Wang, W. Li, Y. Song, W. Xu, Y. Jin, C. Zhang, et al., Monolithic Integrated Flexible Yet Robust Droplet-Based Electricity Generator, Adv. Funct. Mater. 32 (2022). https://doi.org/10.1002/adfm.202206705.

[9] H. Zheng, H. Wu, Z. Yi, Y. Song, W. Xu, X. Yan, et al., Remote-Controlled Droplet Chains-Based Electricity Generators, Adv. Energy Mater. 13 (2023). https://doi.org/10.1002/aenm.202203825.

[10] H. Wu, N. Mendel, S. van der Ham, L. Shui, G. Zhou, F. Mugele, Charge Trapping-Based Electricity Generator (CTEG): An Ultrarobust and High Efficiency Nanogenerator for Energy Harvesting from Water Droplets, Adv. Mater. 32 (2020) 2001699. https://doi.org/10.1002/adma.202001699.

[11] Z.L. Wang, Catch wave power in floating nets, Nature 542 (2017) 159-160. https://doi.org/10.1038/542159a.

[12] A. Siria, M.L. Bocquet, L. Bocquet, New avenues for the large-scale harvesting of blue energy, Nat. Rev. Chem. 1 (2017) 0091. https://doi.org/10.1038/s41570-017-0091.

[13] G. Xue, Y. Xu, T. Ding, J. Li, J. Yin, W. Fei, et al., Water-evaporation-induced electricity with nanostructured carbon materials, Nat. Nanotechnol. 12 (2017) 317-321. https://doi.org/10.1038/nnano.2016.300.

[14] X. Chen, D. Goodnight, Z. Gao, A.H. Cavusoglu, N. Sabharwal, M. DeLay, et al., Scaling up nanoscale water-driven energy conversion into evaporation-driven engines and generators, Nat. commun. 6 (2015) 7346. https://doi.org/10.1038/ncomms8346.

[15] N. Zhang, H. Zhang, W. Xu, H. Gu, S. Ye, H. Zheng, et al., A droplet-based electricity generator with ultrahigh instantaneous output and short charging time, Droplet 1 (2022) 56-64.

https://doi.org/10.1002/dro2.10.
[16] L. Li, X. Wang, W. Deng, J. Yin, X. Li, W. Guo, Hydrovoltaic energy from water droplets: Device configurations, mechanisms, and applications, Droplet 2 (2023) e77. https://doi.org/10.1002/dro2.77.
[17] T.H. Hsu, S. Manakasettharn, J.A. Taylor, T. Krupenkin, Bubbler: A Novel Ultra-High Power Density Energy Harvesting Method Based on Reverse Electrowetting, Sci. Rep. 5 (2015) 16537. https://doi.org/10.1038/srep16537.
[18] K.R. Wijewardhana, T.Z. Shen, J.K. Song, Energy harvesting using air bubbles on hydrophobic surfaces containing embedded charges, Appl. Energy 206 (2017) 432-438. https://doi.org/10.1016/j.apenergy.2017.08.211.
[19] K.R. Wijewardhana, T.K. Ekanayaka, E.N. Jayaweera, A. Shahzad, J.K. Song, Integration of multiple bubble motion active transducers for improving energy-harvesting efficiency, Energy 160 (2018) 648-653. https://doi.org/10.1016/j.energy.2018.07.058.
[20] J. Xiong, G. Thangavel, J. Wang, X. Zhou, P.S. Lee, Self-healable sticky porous elastomer for gas-solid interacted power generation, Sci. Adv. 6 (2020) eabb4246. https://www.science.org/doi/10.1126/sciadv.abb4246.
[21] C. Li, H. Zhang, Y. Wang, X. Liu, A. Ali, Z.Q. Tian, Liquid–Solid Triboelectric Nanogenerator for Bubble Energy Harvesting, Adv. Mater. Technol. 8 (2023) 2201791. https://doi.org/10.1002/admt.202201791.
[22] Y. Dong, S. Xu, C. Zhang, L. Zhang, D. Wang, Y. Xie, et al., Gas-liquid two-phase flow-based triboelectric nanogenerator with ultrahigh output power, Sci. Adv. 8 (2022) eadd0464. https://www.science.org/doi/10.1126/sciadv.add0464.
[23] J. Chen, H. Guo, J. Zheng, Y. Huang, G. Liu, C. Hu, et al., Self-Powered Triboelectric Micro Liquid/Gas Flow Sensor for Microfluidics, ACS Nano 10 (2016) 8104-8112. https://doi.org/10.1021/acsnano.6b04440.
[24] Z. Guan, P. Li, Y. Wen, Y. Du, T. Han, X. Ji, Efficient underwater energy harvesting from bubble-driven pipe flow, Appl. Energy 295 (2021) 116987. https://doi.org/10.1016/j.apenergy.2021.116987.
[25] Z. Guan, P. Li, Y. Wen, Y. Du, Y. Wang, Efficient bubble energy harvesting by promoting pressure potential energy release using helix flow channel, Appl. Energy 328 (2022) 120159. https://doi.org/10.1016/j.apenergy.2022.120159.
[26] Z. Guan, P. Li, Y. Wen, Y. Du, G. Wang, Bubble energy harvesting suitable for weak gas sources using bubble stream release scheme, Appl. Energy 349 (2023) 121620. https://doi.org/10.1016/j.apenergy.2023.121620.
[27] X. Zhang, Q. Zhang, L. Zhang, P. Li, M. Cheng, J. Zhao, et al., Functionally Cooperating Mini-Generator: From Bacterial Fermentation to Electricity, Adv. Funct. Mater. 29 (2019) 1900879. https://doi.org/10.1002/adfm.201900879.
[28] D. Jang, J. Lee, H. Song, H. Park, S.K. Chung. Underwater energy harvesting technology utilizing an optothermally pulsating microbubble. 2018 IEEE Micro Electro Mechanical Systems (MEMS) 2018. p. 685-687. https://doi./10.1109/memsys.2018.8346647
[29] X. Yan, W. Xu, Y. Deng, C. Zhang, H. Zheng, S. Yang, et al., Bubble energy generator, Sci. Adv. 8 (2022) eabo7698. https://www.science.org/doi/10.1126/sciadv.abo7698.
[30] W. Xu, Z. Wang, Fusion of Slippery Interfaces and Transistor-Inspired Architecture for Water Kinetic Energy Harvesting, Joule 4 (2020) 2527-2531.

https://doi.org/10.1016/j.joule.2020.09.007.
[31] S. Krishnan, R. Ayothi, A. Hexemer, J.A. Finlay, K.E. Sohn, R. Perry, et al., Anti-biofouling properties of comblike block copolymers with amphiphilic side chains, Langmuir 22 (2006) 5075-5086. https://doi.org/10.1021/la052978l.
[32] X. Leng, L. Sun, Y. Long, Y. Lu, Bioinspired superwetting materials for water manipulation, Droplet 1 (2022) 139-169. https://doi.org/10.1002/dro2.29.
[33] C. Hao, Y. Liu, X. Chen, J. Li, M. Zhang, Y. Zhao, et al., Bioinspired interfacial materials with enhanced drop mobility: From fundamentals to multifunctional applications, Small 12 (2016) 1825-1839. https://doi.org/10.1002/smll.201503060.
[34] S.S. Kwak, H.J. Yoon, S.W. Kim, Textile-based triboelectric nanogenerators for self-powered wearable electronics, Adv. Funct. Mater. 29 (2019) 1804533. https://doi.org/10.1002/adfm.201804533.
[35] C. Wang, Z. Guo, A comparison between superhydrophobic surfaces (SHS) and slippery liquid-infused porous surfaces (SLIPS) in application, Nanoscale 12 (2020) 22398-22424. https://doi.org/10.1039/d0nr06009g.
[36] A.B. Tesler, S. Kolle, L.H. Prado, I. Thievessen, D. Böhringer, M. Backholm, et al., Long-term stability of aerophilic metallic surfaces underwater, Nat. Mater. (2023) 1-8. https://doi.org/10.1038/s41563-023-01670-6.
[37] C. Yu, X. Zhu, K. Li, M. Cao, L. Jiang, Manipulating Bubbles in Aqueous Environment via a Lubricant-Infused Slippery Surface, Adv. Funct. Mater. 27 (2017) 1701605. https://doi.org/10.1002/adfm.201701605.
[38] K. Han, K. Yong, Overcoming Limitations in Surface Geometry-Driven Bubble Transport: Bidirectional and Unrestricted Movement of an Underwater Gas Bubble Using a Magnetocontrollable Nonwetting Surface, Adv. Funct. Mater. 31 (2021) 2101970. https://doi.org/10.1002/adfm.202101970.
[39] C. Shi, D.Y.C. Chan, Q. Liu, H. Zeng, Probing the Hydrophobic Interaction between Air Bubbles and Partially Hydrophobic Surfaces Using Atomic Force Microscopy, J. Phys. Chem. C 118 (2014) 25000-25008. https://doi.org/10.1021/jp507164c.
[40] A.K. Epstein, T.S. Wong, R.A. Belisle, E.M. Boggs, J. Aizenberg, Liquid-infused structured surfaces with exceptional anti-biofouling performance, Proc. Natl. Acad. Sci. 109 (2012) 13182-13187. https://doi.org/10.1073/pnas.1201973109.
[41] C.S. Ware, T. Smith Palmer, S. Peppou Chapman, L.R. Scarratt, E.M. Humphries, D. Balzer, et al., Marine antifouling behavior of lubricant-infused nanowrinkled polymeric surfaces, ACS Appl. Mater. Interfaces 10 (2018) 4173-4182. https://doi.org/10.1021/acsami.7b14736.
[42] T.S. Wong, S.H. Kang, S.K.Y. Tang, E.J. Smythe, B.D. Hatton, A. Grinthal, et al., Bioinspired self-repairing slippery surfaces with pressure-stable omniphobicity, Nature 477 (2011) 443-447. https://doi.org/10.1038/nature10447.
[43] Z. Wang, L. Scheres, H. Xia, H. Zuilhof, Developments and challenges in self-healing antifouling materials, Adv. Funct. Mater. 30 (2020) 1908098. https://doi.org/10.1002/adfm.201908098.
[44] W. Xu, X. Zhou, C. Hao, H. Zheng, Y. Liu, X. Yan, et al., SLIPS-TENG: robust triboelectric nanogenerator with optical and charge transparency using a slippery interface, Natl. Sci. Rev. 6 (2019) 540-550. https://doi.org/10.1093/nsr/nwz025.

[45] H. Wu, S. Wang, Z. Wang, Y. Zi, Achieving ultrahigh instantaneous power density of 10 MW/m(2) by leveraging the opposite-charge-enhanced transistor-like triboelectric nanogenerator (OCT-TENG), Nat. Commun. 12 (2021) 5470. https://doi.org/10.1038/s41467-021-25753-7.
[46] Y. Song, W. Xu, Y. Liu, H. Zheng, M. Cui, Y. Zhou, et al., Achieving ultra-stable and superior electricity generation by integrating transistor-like design with lubricant armor, Innovation 3 (2022) 100301. https://doi.org/10.1016/j.xinn.2022.100301.